



An empirical zenith wet delay correction model using piecewise height functions

YiBin Yao^{1,2,3}, YuFeng Hu^{1*}

¹*School of Geodesy and Geomatics, Wuhan University, 129 Luoyu Road, Wuhan 430079, China.*

²*Key Laboratory of Geospace Environment and Geodesy, Ministry of Education, Wuhan University,
129 Luoyu Road, Wuhan 430079, China*

³*Collaborative Innovation Center for Geospatial Technology, 129 Luoyu Road, Wuhan 430079,
China*

**Corresponding to: yfhu@whu.edu.cn*

Abstract—Tropospheric delay is an important error source in space geodetic techniques. The temporal and spatial variations of the zenith wet delay (ZWD) are very large, and thus limit the accuracy of tropospheric delay modelling. Thus it is worthwhile undertaking research aimed at constructing a precise ZWD model. Traditional tropospheric modelling methods do not consider the effects of different heights on ZWD. Based on the analysis of vertical variations of ZWD, we divided the troposphere into three height intervals: below 2 km, 2 km to 5 km, and 5 km to 10 km, and determined the fitting functions for the ZWD within these height intervals. The global ZWD model HZWD, which considers the periodic variations of ZWD with a spatial resolution of $5^\circ \times 5^\circ$, is established using the ECMWF ZWD profiles from 2001 to 2010. Validated by the ECMWF ZWD data in 2015, the precisions of the ZWD estimation in the HZWD model over the three height intervals are improved by 1.4 mm, 0.9 mm, and 1.2 mm, respectively, compared to that of the currently best GPT2w model (23.8 mm, 13.1 mm, and 2.6 mm). The test results from ZWD data from 318 radiosonde stations show that the root mean square (RMS) error in the HZWD model over the three height intervals was reduced by 2%, 5%, and 33%, respectively, compared to the GPT2w model (30.1 mm, 15.8 mm, and 3.5 mm) over the three height intervals. In addition, the spatial and temporal stabilities of the HZWD model are higher than those of GPT2w and UNB3m.



29

30 **Index Terms**—Tropospheric delay, zenith wet delay, vertical variations, height dividing,
31 HZWD model.

32

33 **1 Introduction**

34 The radio waves experience propagation delays when passing through the neutral
35 atmosphere (primarily the troposphere), which are known as the tropospheric delays.
36 The tropospheric delay is one of the main error source in space geodetic techniques. In
37 the processing of the space geodetic data, the tropospheric delay along the propagation
38 path is generally expressed as the product of zenith tropospheric delay (ZTD) and
39 mapping function (MF). The ZTD is divided into a zenith hydrostatic delay (ZHD) and
40 a zenith wet delay (ZWD) (Davis *et al.*, 1985), and the ZHD can be accurately
41 determined using pressure observations. Unlike the ZHD, the ZWD is difficult to
42 calculate accurately due to the high spatio-temporal variation in water vapour, thus
43 making itself the main factor influencing tropospheric delay correction.

44 The traditional Saastamoinen model (1972) and Hopfield model (1971)
45 approximate the ZWD with temperature and water vapour pressure observations.
46 Without considering the vertical distribution of water vapour, the stability and reliability
47 of their ZWD estimates are poor. Moreover, both models are highly dependent on
48 meteorological data, which greatly limits their application in wide area augmentation
49 and real-time navigation and positioning. Therefore, non-meteorological parameters-
50 based models were proposed as practical conditions required. The RTCA-MOPS (2016),
51 designed by the US Wide Area Augmentation System (Collins *et al.*, 1996), estimates
52 ZWD by using the latitude band parameters table. The modified RTCA-MOPS model
53 – called UNB3m (Leandro, 2006) – uses relative humidity as a parameter instead of the
54 water vapour pressure to calculate the ZWD, effectively improving the precision of
55 ZWD estimation compared with previous model versions, but the model deviation is
56 increased when the height exceeds 2 km. The TropGrid model (Krueger *et al.*, 2004,
57 2005) provides the meteorological parameters needed to calculate tropospheric delay in



the form of $1^\circ \times 1^\circ$ grid. The TropGrid model calculates ZWD with modelled water vapour pressure and weighted mean temperature data, while the TropGrid2 model (Schüller, 2014) directly models ZWD and uses the exponential function to describe the variation of ZWD with respect to height, resulting in a precision improvement. Based on the GPT2 model (Lagler *et al.*, 2013), the GPT2w model (Běhm *et al.*, 2015) adds weighted mean temperature and a vapour pressure decrease factor realised as a global grid to estimate ZWD by using the Askne and Nordius formula (Askne & Nordius, 1987). The GPT2w model has the best performance with regard to ZWD estimation compared to other commonly used models (Möller *et al.*, 2014).

The water vapour changes rapidly with respect to height, and the trends in water vapour at different heights vary, so the wet delay with direct relation to water vapour has complex spatio-temporal variations in the vertical direction. The aforementioned troposphere models are all based on a fixed height (average sea level or surface height) and use only a single decrease factor to describe the variation of water vapour or wet delay with respect to height, which makes it difficult to allow for the vertical distribution differences in water vapour (or wet delay) in the upper troposphere. In the course of aircraft dynamic navigation and positioning, it is necessary to correct the wet delay at different heights, which is obviously difficult for the aforementioned models. Based on the analysis of the characteristics of the ZWD profile, an empirical ZWD model, named HZWD, is established based on three functions applicable within corresponding height intervals, and the model precision is verified by European Centre for Medium-Range Weather Forecast (ECMWF) reanalysis data as well as radiosonde data.

2 Vertical variations of ZWD

ZWD is defined as the integral of the wet refractivity along the vertical profile above the station:

$$ZWD = 10^{-6} \int_H^\infty N_w dh = 10^{-6} \int_H^\infty (k'_2 \frac{e}{T} + k_3 \frac{e}{T^2}) dh \quad (1)$$



86 In equation (1), N_w is the wet refractivity; e is the water vapour pressure in hPa;
 87 T is the temperature in Kelvin; k'_2 is 17 K/hPa and k_3 is 377600 K²/hPa (Bevis *et al.*,
 88 1992). It can be seen from equation (1) that ZWD changes with height, vapour pressure
 89 and temperature. The ZWD will decrease with increasing height due to the shorter
 90 integral length. The accurate ZWD calculation requires profiles of water vapour
 91 pressure and temperature, which are difficult to access in practical applications (such
 92 as aircraft navigation and positioning and wide area augmentation). Therefore, it is
 93 necessary to develop an empirical ZWD model with high precision. The temperature
 94 roughly decreases linearly with increasing height in the troposphere, while the change
 95 in water vapour is more variable, so the water vapour is the main determinant of vertical
 96 variation of ZWD. In the following content, we used the meteorological data profile of
 97 ERA-Interim pressure levels provided by ECMWF to analyse the vertical variation
 98 characteristics of ZWD and explore a suitable fitting function capable of describing the
 99 changes in ZWD with respect to height.

100 ERA-Interim can provide data at 0:00, 6:00, 12:00, and 18:00 UTC daily with a
 101 spatial resolution of not more than $0.125^\circ \times 0.125^\circ$ and 37 pressure levels. The highest
 102 level data come from a height of approximately 50 km, covering almost the entire
 103 troposphere and stratosphere. We used the temperature, the geopotential height, and the
 104 specific humidity provided by the ERA-Interim pressure levels data, and the discretised
 105 form of equation (1), to calculate the ZWD for each level height:

$$106 \quad \begin{cases} e_i = q_i \times P_i / (0.622 + 0.378 \times q_i) \\ N_{w_i} = k'_2 \frac{e_i}{T_i} + k_3 \frac{e_i}{T_i^2} \\ ZWD = 10^{-6} \sum_i^{36} \frac{N_{w_i} + N_{w_{i+1}}}{2} \cdot (h_{i+1} - h_i) \end{cases} \quad (2)$$

107 In equation (2), e is the water vapour pressure in hPa; q is the specific humidity in g/g;
 108 P is the pressure in hPa; T is the temperature in kelvin; k'_2 and k_3 are empirical
 109 constants same as equation (1); h is the geopotential height in meters. From equation



(2), we can see that the ZWD at specific level height is the sum of the ZWD portions in all layers above the specific level height. Figure 1 shows the water vapour pressure and ZWD profiles at a grid point (0 °N, 0 °E) at 12:00 UTC on 1 January, 2010. From Figure 1, it can be seen that the downward trend in the water vapour pressure varies significantly with height, and the decrease factor is different across different height intervals. The changes in ZWD with respect to height are similar to that of the water vapour pressure with respect to height: the decay is fastest up to a few kilometres height and slows down with increasing height; the ZWD values are close to zero after 10 km. Zhao *et al.* (2014) showed that about 50% of the water vapour content is concentrated within 1.5 km of the surface and less than 10% of the water vapour content remains above 5 km, leading to different ZWD decay rates within different height intervals. These results are basically consistent with our experiment results. Figure 2a shows the variation of ZWD vertical gradients with respect to height. From Figure 2a, it can be seen that the trends in ZWD vertical gradients at different height intervals are obviously different. Specifically, the linear fit of the ZWD gradients with height below 2 km shows a great agreement with an R square value of 0.99 (Figure 2b). Thus we can come to a conclusion: ZWD gradients roughly change linearly below 2 km; and from 2 km to 5 km, and 5 km to 10 km, the ZWD gradients vary non-linearly.

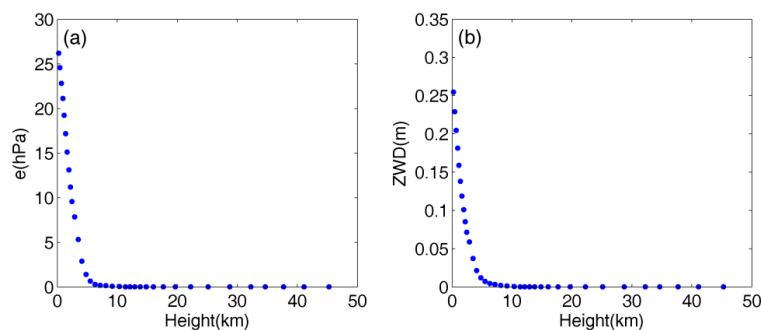
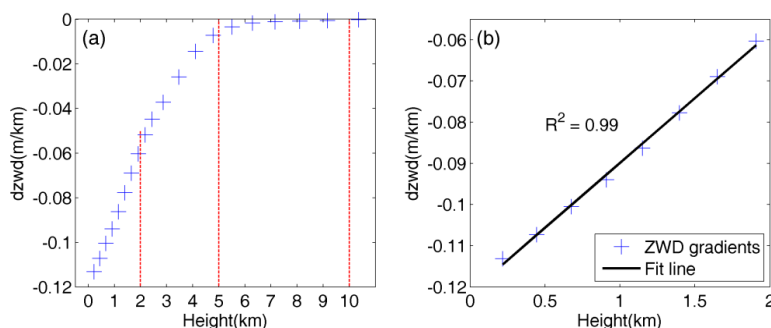


Figure 1 Water vapour pressure (a) and ZWD (b) versus height.



131

132 Figure 2 ZWD vertical gradients with respect to height (a) and linear fit with height below 2 km

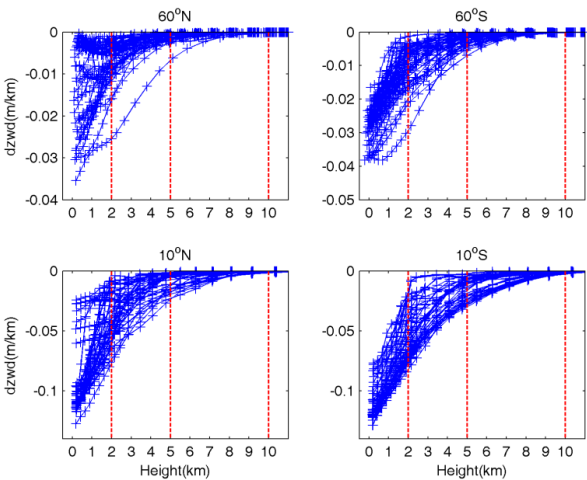
133

(b).

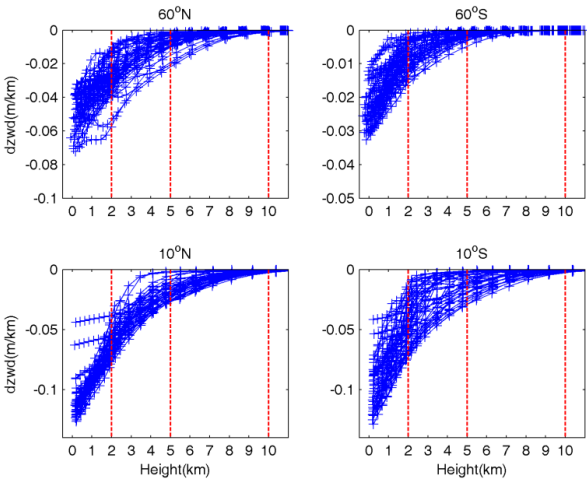
134 Figure 3 shows the ZWD vertical gradients with respect to height at grid points in
 135 different latitude bands. Figure 4 shows the similar ZWD vertical gradients as Figure 3
 136 but for different season. The variations are similar to those in Figure 2a, which show
 137 trend changes at about 2 km and 5 km. It is worth noting that the ZWD gradients at high
 138 latitudes are much larger and water vapour is more variable than at low latitudes,
 139 resulting from the fact that the water vapour at high latitudes are more variable. In
 140 addition, the ZWD gradient trends in the southern hemisphere are significant. In
 141 contrast, the ZWD gradients in the northern hemisphere are slightly complicated with
 142 respect to height: the reason for this may be that the southern hemisphere is mostly
 143 oceanic while the northern hemisphere has many seacoasts. The terrain complexity in
 144 the northern hemisphere contributes to the disturbances in the ZWD gradient in specific
 145 areas. According to the vertical variation characteristics of ZWD, we divided the
 146 troposphere into three height intervals: below 2 km, 2 km to 5 km, and 5 km to 10 km,
 147 and assumed 10 km as the empirical tropopause beyond which the ZWD is assumed to
 148 be zero. For ZWD fitting with respect to height, TropGrid2 and GPT2w use exponential
 149 functions, while some scholars have also used a polynomial to describe the tropospheric
 150 delay with respect to height (Song *et al.*, 2011). We used both polynomial and
 151 exponential functions to fit the variation trend of the ZWD with respect to height in the
 152 three selected intervals, respectively. The results showed that the quadratic polynomial
 153 used under 2 km, and exponential functions between 2 km and 5 km, and 5 km to 10



154 km gave the best fits. The combination of the quadratic polynomial and exponential
155 functions for different height intervals is termed piecewise height functions. Table 1
156 summarises the global fitting statistics of different fit functions, demonstrating the
157 superiority of piecewise height functions to the single polynomial function and single
158 exponential function.



159
160 Figure 3 ZWD gradients with respect to height at grid points in different latitude bands (12:00
161 UTC, 1 January, 2010).



162
163 Figure 4 ZWD gradients with respect to height at grid points in different latitude bands (12:00
164 UTC, 1 July, 2010).



Table 1. Fitting RMSs of piecewise height functions, single quadratic polynomial function, and single exponential function (unit: mm).

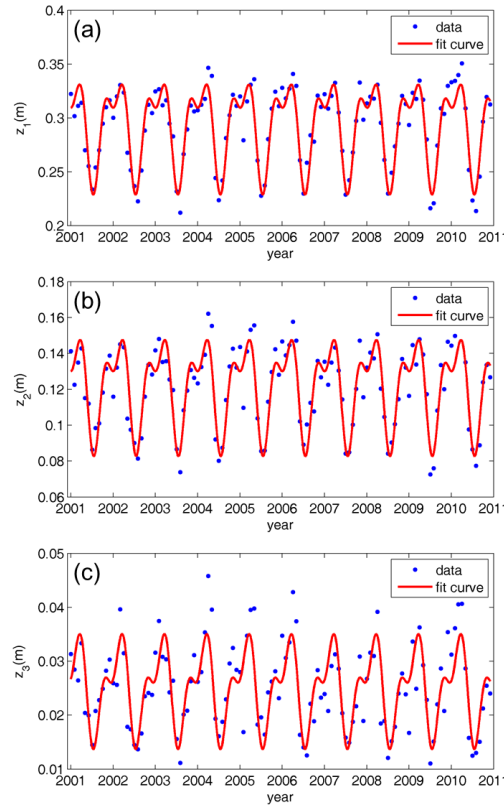
	< 2 km	2 km to 5 km	5 km to 10 km
Piecewise height functions	0.2	1.0	0.2
Quadratic polynomial	5.9	3.8	6.5
Exponential	2.3	2.2	1.0

3 The HZWD model

From the above analysis of ZWD vertical variation and fitting, the piecewise height functions of the proposed HZWD model are:

$$ZWD(B, L, H) = \begin{cases} z_1 + a_1 \cdot h + a_2 \cdot h^2 & h < 2000 \text{ m} \\ z_2 \cdot \exp\{\beta_2 \cdot (h - 2000)\} & 2000 \text{ m} \leq h < 5000 \text{ m} \\ z_3 \cdot \exp\{\beta_3 \cdot (h - 5000)\} & 5000 \text{ m} \leq h \leq 10000 \text{ m} \\ 0 & h > 10000 \text{ m} \end{cases} \quad (3)$$

In equation (3), B is the latitude in degrees; L is the longitude in degrees; H is the height in meters; function coefficients z_1, z_2 and z_3 can be regarded as the ZWD at the height of 0 km, 2 km and 5 km, respectively. We used the monthly mean profiles of ERA-Interim pressure levels from 2001 to 2010 with a horizontal resolution of $5^\circ \times 5^\circ$ for ZWD modelling. The ZWD profiles calculated for each grid point are fitted by equation (3) to obtain the time series of the corresponding function coefficients: $z_1, a_1, a_2, z_2, \beta_2, z_3$, and β_3 . Jin *et al.* (2007) found that the tropospheric delay has notable seasonal variations, mainly on annual and semi-annual cycles. Song *et al.* (2011) and Zhao *et al.* (2014) considered the temporal features of function coefficients in their troposphere models. We used the ten-year time series of those coefficients obtained to analyse their temporal variations. Figure 5 shows the time series and cycle fitting results of the function coefficients z_1, z_2 , and z_3 at grid point ($0^\circ\text{N}, 0^\circ\text{E}$). Figure 5 shows that the time series of the function coefficients z_1, z_2 , and z_3 have a significant characteristic annual cycle, and the semi-annual cycle is small but nevertheless obvious.



187

188 Figure 5 Time series and cycle fitting results of function coefficients z_1 (a), z_2 (b), and z_3 (c).

189 Therefore, taking the annual, and semi-annual, cycles into consideration, we used
 190 equation (4) to fit the function coefficients derived from equation (3) to temporal
 191 parameters for each grid point (Břhm *et al.*, 2015):

$$r(t) = A_0 + A_1 \cos\left(\frac{doy}{365.25} 2\pi\right) + B_1 \sin\left(\frac{doy}{365.25} 2\pi\right) + A_2 \cos\left(\frac{doy}{365.25} 4\pi\right) + B_2 \sin\left(\frac{doy}{365.25} 4\pi\right) \quad (4)$$

192

193 In equation (4), A_0 is the annual mean; A_1 and B_1 are the annual cycle
 194 parameters; A_2 and B_2 are the semi-annual cycle parameters; and *doy* is the day of
 195 the year. It should be noted that the fitting results of coefficients a_2 , β_2 , and β_3
 196 showed that all their annual means, and annual, and semi-annual, amplitudes are small.



197 However, below 2 km, the lack of cycle terms in a_2 would cause centimetre level error
 198 in the ZWD estimates, so these terms have been retained. For β_2 and β_3 , ZWD itself
 199 is small at heights above 2 km, so the annual mean suffices for a desirable ZWD
 200 estimate. The experiment revealed that the loss of accuracy due to the lack of annual
 201 and semi-annual terms in β_2 and β_3 for the ZWD estimates is less than 0.1 mm.
 202 Therefore, only the annual means are retained for these two coefficients.

203 Figure 6 shows the global distributions of annual means of model coefficients z_1 ,
 204 z_2 , and z_3 . From Figure 6 we can see that the extremum of ZWD annual means at 0 m
 205 height occur near the equator and the maximum exceeds 0.36 m. The ZWD annual
 206 means decrease with increasing latitude. The distributions of ZWD annual means at 2
 207 km and 5 km heights are similar to that at 0 m, but the areas with the large values near
 208 the equator decrease in extent and the ZWD distributions tend to be uniform, indicating
 209 that the water vapour content near the equator is greater than that in other regions, and
 210 the ZWD value is also larger in low altitude regions. As the height increases, the
 211 difference in water vapour content or ZWD, between the equator and other areas begins
 212 to decrease, but remains significant. Overall, there are some differences in the ZWD
 213 distribution at different heights, and it is necessary to model the spatio-temporal
 214 variations of ZWD at different heights.

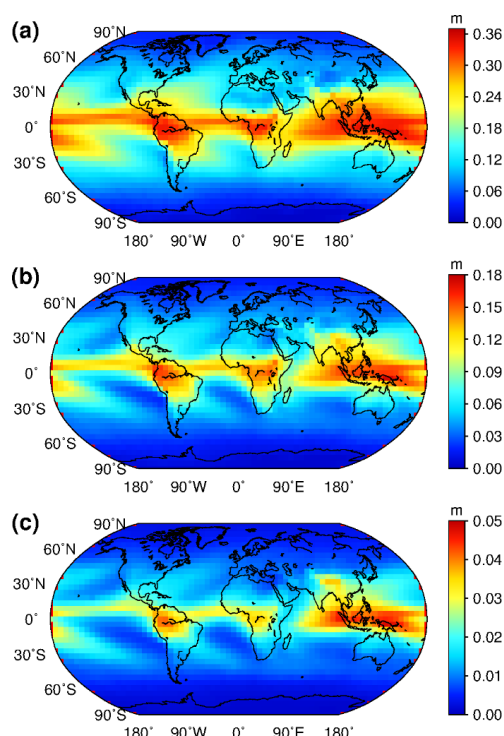


Figure 6 Global distributions of annual means of model coefficients z_1 (a), z_2 (b), and z_3 (c).

After the fitting processes involving equations (3) and (4), the global ZWD model HZWD, using piecewise height functions, is established. The spatial resolution of the HZWD model is $5^\circ \times 5^\circ$. For each grid point, there are 27 parameters which are stored in text format. When the HZWD model is applied, the four grid points surrounding the station are determined according to the horizontal position (latitude and longitude) of the station, and then the model coefficients of the corresponding height intervals at the four selected points are calculated according to equation (4). The ZWD of the four grid points are extrapolated to the station height by using equation (3), and finally the ZWD at the station location is obtained by using bilinear interpolation. The HZWD model only needs time, latitude, longitude, and height as input parameters. It can calculate ZWD without meteorological data, and can provide wet delay correction products for navigation and positioning at different heights.



231 4 Validation and analysis of the HZWD model

232 To test the precision of HZWD model and analyse the model correction
 233 performance compared to other troposphere models, we used the ERA-Interim pressure
 234 levels data and radiosonde data from the year 2015 as external data sources, and
 235 compared the results with the commonly used models UNB3m and GPT2w. The
 236 parameters used for the validation are bias and RMS expressed as:

$$237 \quad bias = \frac{1}{n} \sum_{i=1}^n (ZWD_i^M - ZWD_i^0) \quad (5)$$

$$238 \quad RMS = \sqrt{\frac{1}{n} \sum_{i=1}^n (ZWD_i^M - ZWD_i^0)^2} \quad (6)$$

239 In equation (5) and (6), ZWD_i^M is the value estimated by the model and ZWD_i^0
 240 is the reference value.

241 For the UNB3m model, the ZWD at mean sea level (MSL) is first calculated, then
 242 a vertical correction is applied to transform the ZWD to the target height. The formulae
 243 are (Leandro *et al.*, 2006):

$$244 \quad \begin{cases} ZWD_0 = 10^{-6} \frac{(T_m k'_2 + k_3) R_d}{g_m (\lambda + 1) - \beta R_d} \cdot \frac{e_0}{T_0} \\ ZWD = ZWD_0 \left(1 - \frac{\beta H}{T_0} \right)^{\frac{(\lambda+1)g}{\beta R_d} - 1} \end{cases} \quad (7)$$

245 where T_m is the weighted mean temperature; R_d is the specific gas constant for dry
 246 air; g_m is the gravity acceleration at the mass centre of the vertical column of the
 247 atmosphere; β and λ are the temperature lapse rate and water vapour decrease
 248 factor, respectively.

249 For the GPT2w model, the modelled meteorological parameters at the four grid
 250 points surrounding the target location are extrapolated vertically to the desired height,
 251 then the Askne and Nordius formula (8) is used to calculate the wet delays at those base
 252 points: finally the wet delays are interpolated to the observation site in horizontal
 253 direction to get the target ZWD. It should be noted that the GPT2w model provides both
 254 $1^\circ \times 1^\circ$ and $5^\circ \times 5^\circ$ resolution versions. Since the horizontal resolution of HZWD model



is $5^\circ \times 5^\circ$, we used the GPT2w model with the same resolution for validation.

$$ZWD = 10^{-6} \cdot (k'_2 + \frac{k'_3}{T_m}) \cdot \frac{R_d e}{(\lambda + 1) g_m} \quad (8)$$

4.1 Validation with ECMWF data

Modelling of the HZWD model is based on the monthly mean profiles of ERA-Interim pressure levels data from 2001 to 2010, while we used the ERA-Interim pressure levels data with the full time resolution of 6 hours in 2015 for the model validation. Regarding the ZWD profiles calculated from these data as reference values, we calculated the global annual average bias and RMS error of the ZWD for three models (HZWD, GPT2w, and UNB3m) within the three height intervals: below 2 km, 2 km to 5 km, and 5 km to 10 km (Table 2).

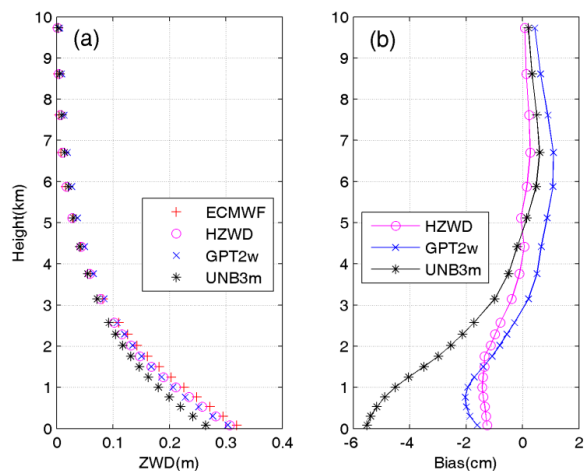
Table 2 Error statistics for the three models compared to the 2015 ECMWF data (unit: mm).

	< 2 km		2 km to 5 km		5 km to 10 km	
	bias	RMS	bias	RMS	bias	RMS
HZWD	-2.0	23.8	-1.4	13.1	0.0	2.6
GPT2w	-0.1	25.2	2.5	14.0	2.2	3.8
UNB3m	16.6	41.4	10.9	22.7	3.5	5.8

From Table 2, it can be seen that the HZWD model is the most accurate model across all three intervals, followed by the GPT2w model, and the UNB3m model has the worst performance. The annual average biases of the HZWD model are lower than that of the GPT2w model and the UNB3m model except below 2 km. Compared with the RMS errors in the GPT2w model, those of the HZWD model are decreased by 1.4 mm, 0.9 mm, and 1.2 mm within the three height intervals, corresponding to improvements of about 6%, 6%, and 32%, respectively. The correction performance improvement from 5 km to 10 km height is particularly evident. Figure 7a shows the ECMWF ZWD profile and the ZWD profiles of the three models at 12:00 UTC on 1 January, 2015 at a representative grid point (0°N , 20°E). More clearly, Figure 7b shows the differences between the ZWD profiles of the three models and ECMWF ZWD profile at different heights. It can be seen that HZWD is the most stable model, showing



278 the best agreement with the ECMWF ZWD data, which is superior to both the GPT2w,
279 and the UNB3m, models.
280



281
282 Figure 7 The ZWD profiles of ECMWF and the three models (a) and corresponding biases (b).
283 The variation of the troposphere has a strong correlation with latitude. To analyse
284 the correction performances of the three models in different regions around the world,
285 we calculated the three models' errors in different latitude bands (10° intervals). Figures
286 8 and 9 show the correction performances at different latitudes. It can be seen from
287 Figure 8 that the bias of the UNB3m model is basically positive in the three height
288 intervals, indicating that its ZWD estimates are relatively large compared to the
289 ECMWF data. Moreover, the bias in the southern hemisphere is significantly larger than
290 that in the northern hemisphere, indicating systematic deviations in the southern
291 hemisphere. Both the GPT2w model and the HZWD model have large biases in the low
292 latitudes. The biases of the GPT2w model are positive from 2 km to 5 km and 5 km to
293 10 km height, indicating that the ZWD is overestimated by the GPT2w model with
294 increasing height. For the HZWD model, the bias in each latitude band is relatively
295 small with few exceptions, resulting in a global average bias close to zero (see Table 2).
296 The annual average bias indicates the degree of deviation between the ZWD
297 estimates of the three models and the reference ECMWF data, while the RMS error
298 reflects the reliability and stability of the model, *i.e.*, the model precision. It can be seen



299 from Figure 9 that the precision of HZWD model is significantly better than that of the
300 UNB3m model across the three height intervals and all latitude bands, which is better
301 than GPT2w model in general. The precision of the three models declines with
302 decreasing latitude, because the active change of water vapour in these areas limits the
303 precision of the model. Corresponding to Figure 8, the errors in UNB3m are asymmetric:
304 the main reason for this is that the meteorological parameters of UNB3m are
305 interpolated from the coarse look-up table with a latitude interval of 15° and UNB3m
306 does not consider the longitudinal variations of any meteorological elements. It should
307 be pointed out that the UNB3m model is based on the simple symmetric assumption of
308 the northern and southern hemispheres, and its modelling data source only comes from
309 the atmospheric data collected over North America, which leads to poor precision in
310 the southern hemisphere, especially in the high latitudes thereof.

311 Summarising the distributions of bias and RMS error across different latitude
312 bands, we can see that the HZWD model performs best with the ECMWF data as
313 reference values. Compared with the models GPT2w and UNB3m, the HZWD model
314 basically eliminates systematic error in the 5 km to 10 km height interval and the
315 correction performance is stable at all heights and regions. To investigate the model's
316 performance over time, the Figure 10 shows the time series of biases for the three
317 models at 6-hour intervals throughout the year 2015 at grid point (0°N , 20°E). We can
318 see that the HZWD model has the best overall performances within the three height
319 intervals over the year 2015. We noticed the significantly large biases for all three
320 models across all three height intervals around the day 19 and day 195 of 2015. This
321 can be attributed to the sharp short-term ZWD variations in the equator area. The short-
322 term variations are hardly accounted for by all three models which only consider the
323 seasonal variations of ZWD. Moreover, the GPT2w model has the worst performance
324 from 5 km to 10 km height, showing significant overestimates of the ZWD. The poor
325 performance of GPT2w at high heights in the equator area is also identified by Figure
326 8 and Figure 9.

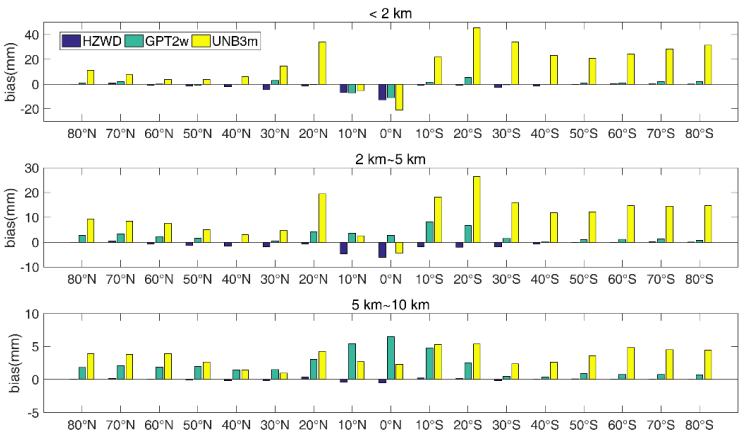


Figure 8 Bias comparisons between the three models in different latitude bands.

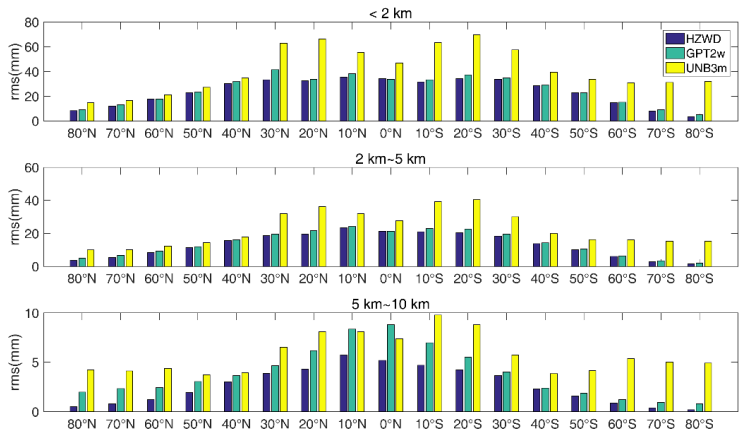


Figure 9 RMS error comparisons between the three models in different latitude bands.

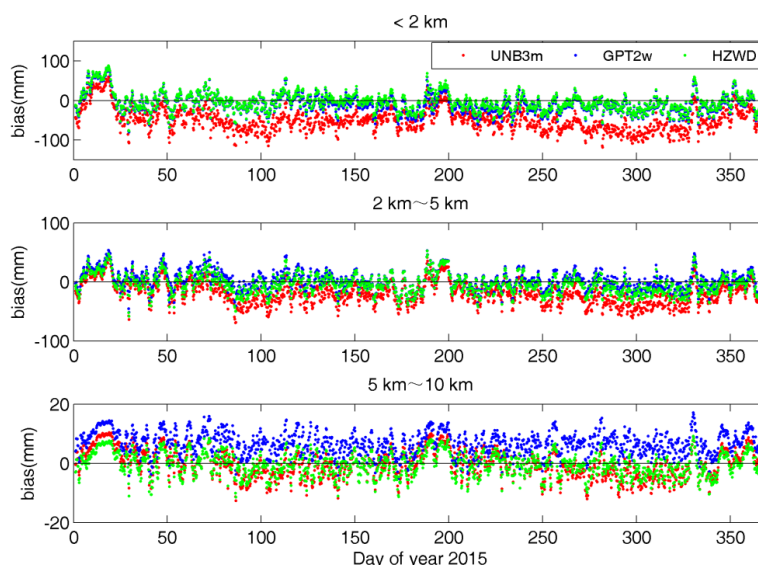


Figure 10 Biases in ZWD estimates of the three models compared to the ECMWF data over the year 2015 at grid point (0°N, 20°E).

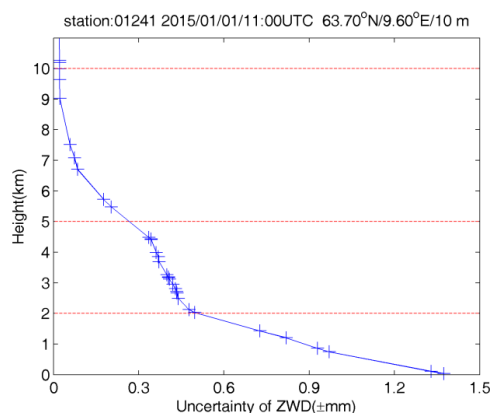
4.2 Validation with radiosonde data

A radiosonde is used in a sounding technique that regularly releases balloons to collect atmospheric meteorological data at different heights: it can obtain profiles of various meteorological data with high accuracy. At present, the Integrated Global Radiosonde Archive (IGRA) website (<ftp://ftp.ncdc.noaa.gov/pub/data/igra/>) provides free downloads of global radiosonde data. We used radiosonde data from 318 stations collected in 2015 to test the HZWD model. After data pre-processing, the data with gross errors have been removed and a total of 163,671 radiosonde data epochs remained. With the provided profiles of geopotential height, temperature, and water vapour pressure, the data form of the radiosonde data are very similar to the ECMWF pressure level data, thus the radiosonde ZWDs can be calculated using the same method by equation (2). Before the validation, we conducted an assessment of the uncertainty of ZWD derived from radiosonde data. Rozsa (2014) showed that the uncertainty of ZWD is ± 1.5 mm in case of the Vaisala RS-92 radiosondes in Central and Eastern Europe. However, this uncertainty is only valid for the ZWD calculated from the height of



lowest layer and is limited to Europe area. Using the same uncertainties of radiosonde meteorological data given by the technical specification of the radiosonde (Vaisala 2010) and the algorithm proposed by Rozsa (2014), we calculated the ZWD uncertainty for all heights in all radiosonde stations. Figure 11 shows the uncertainty of ZWD with respect to the height for radiosonde station 01241 located in Orland, Norway (63.70°N/9.60°E/10 m). We can see that the uncertainty of ZWD is less than ± 1.5 mm near height of 0 m and decrease quickly with increasing height. The global mean uncertainties of ZWD of all stations in the three height intervals are ± 1.3 mm, ± 0.7 mm and ± 0.2 mm, respectively, indicating the high accuracy of ZWD derived from radiosonde data.

361



362

363 Figure 11 Uncertainty of ZWD with respect to height at station 01241.

364 Taking the radiosonde ZWDs as reference ZWD values, we validated the ZWDs
 365 from models HZWD, GPT2w and UNB3m. Table 3 shows the statistical results of the
 366 three models. It can be seen from Table 3 that the HZWD model has the best overall
 367 stability of the average bias and RMS error indicating the best precision, and the
 368 UNB3m model is the worst. Compared with the GPT2w model, the RMS errors in
 369 HZWD in the three height intervals are reduced by 0.6 mm, 0.9 mm, and 1.7 mm, which
 370 equates to precision improvements of 2%, 5%, and 33%, respectively. Taking the
 371 uncertainty of radiosonde ZWD into account, the improvement of HZWD model over
 372 GPT2w model below 2 km seem to be insignificant. However, the validation is based



on the same radiosonde ZWD values and the RMS error of ZWD of HZWD is smaller, thus we can reasonably expect that the ZWD of HZWD is closer to true ZWD value than the ZWD of GPT2w in spite of the uncertainty of radiosonde ZWD. It is worth noting that the bias and RMS error of the HZWD model and the GPT2w model are both larger than those of the results from ECMWF data in Table 2. The reason is that the HZWD model and the GPT2w model are based on ECMWF data, thus the test results with radiosonde data are slightly worse than those using ECMWF data. On the contrary, the bias of the UNB3m model decreases, and the RMS error between 2 km and 5 km, and 5 km and 10 km, are less than those in Table 2. It may be due to the fact that most of the radiosonde stations are in the northern hemisphere, accounting for more than 60% (192/318) of the total, which has a positive impact on the test results for UNB3m model based on North American meteorological data.

Figure 12 shows the global distributions of bias for the three models within the three height intervals, and Figure 13 shows the global distributions of RMS error for the three models. As can be seen from Figure 12, the three models show a poorer performance in low-latitude areas than in mid- and high-latitude areas for all height intervals, similar to the results of in Section 4.1. Within the 5 km to 10 km interval, the bias of the GPT2w model is large and positive in the equatorial region, indicating that the ZWD of the GPT2w in this height is significantly overestimated, and the global bias of the UNB3m model in this height interval is positive, also indicating an overestimate of the ZWD in the UNB3m model. The bias of the HZWD model does not show obvious regional differences with respect to height, and the overall distribution of HZWD model bias has no tendency to either the positive or negative. Figure 13 further illustrates the precision of the HZWD model. The global RMS error distributions of HZWD model are similar to that of GPT2w model below 2 km and between 2 km and 5 km, but the precision of the HZWD model is slightly better. Combining this with the bias distribution of the GPT2w model in Figure 12, the GPT2w model also has a large RMS error near the equator in the 5 km to 10 km interval, which shows that the GPT2w model is unstable at high height in low-latitude areas. The precision of the UNB3m model is poorer than that of both the HZWD, and GPT2w, models. Below 2 km, the UNB3m



model reaches decimetre-level precision near the equator, and even exceeds 12 cm in
some areas: the distribution of north-south heterogeneity remains obvious.
Table 3 Error statistics for the three models validated by 2015 radiosonde data (unit: mm).

	< 2 km		2 km to 5 km		5 km to 10 km	
	bias	RMS	bias	RMS	bias	RMS
HZWD	-3.6	30.1	-2.0	15.8	0.1	3.5
GPT2w	-3.2	30.7	3.5	16.7	3.3	5.2
UNB3m	5.9	46.0	6.2	23.1	2.6	5.7

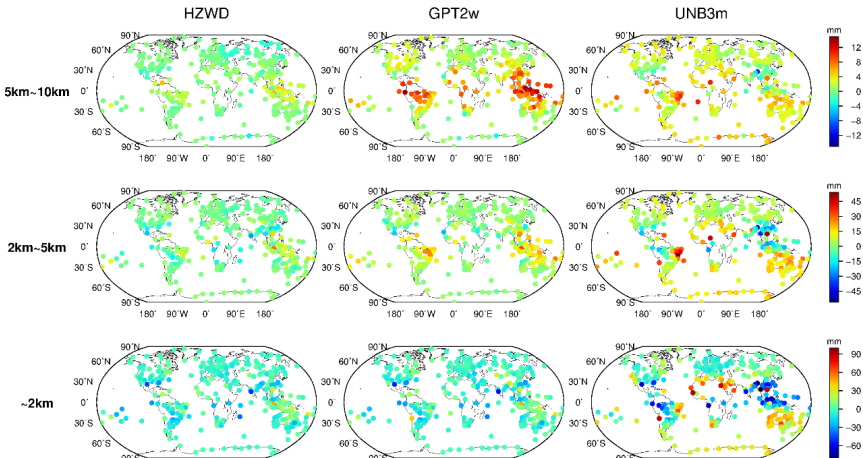
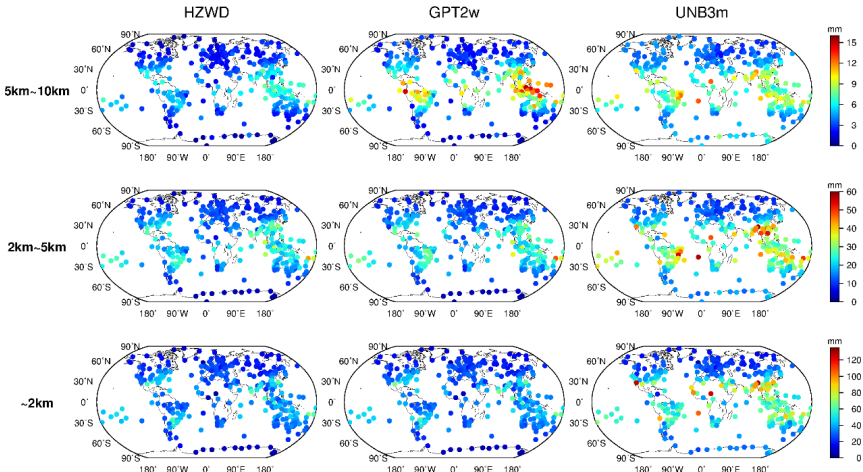


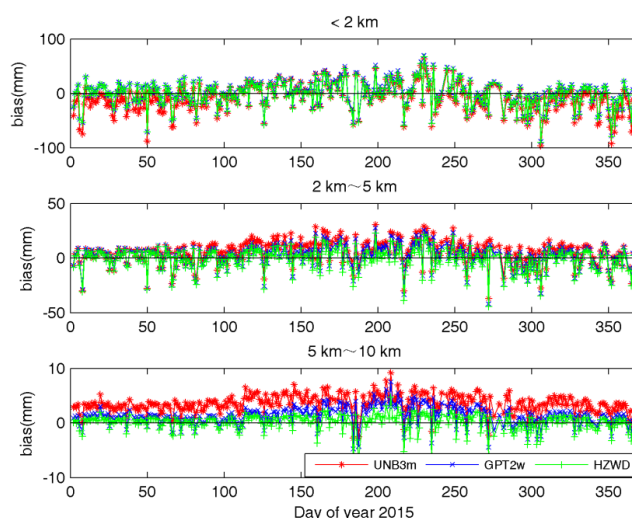
Figure 12 Global distributions of bias for the three models compared to 2015 radiosonde data.





410 Figure 13 Global distributions of RMS error for the three models compared to 2015 radiosonde
 411 data.

412 These results validate the spatial stability of the precision of the HZWD model,
 413 furthermore the temporal stability of the model precision is verified next. Figure 14
 414 shows the results of ZWD corrections of the three models for the radiosonde station
 415 01241 for the whole of 2015. It can be seen from Figure 14 that the HZWD model and
 416 the GPT2w model are relatively stable throughout the year, while the correction
 417 performance of the UNB3m model in 2015 is worse than those of the HZWD and
 418 GPT2w models. The probable reason for this is that the UNB3m model only takes into
 419 account the annual variations in the metrological elements with a fixed phase, resulting
 420 in precision instability throughout the year. The improvement performance arising from
 421 use of the HZWD model, compared to that arising from use of the GPT2w model, is
 422 more apparent with increasing height: this shows that modelling ZWD piecewise with
 423 height can effectively approximate the real ZWD profile and improve the precision of
 424 ZWD estimation.



425
 426 Figure 14 Biases in ZWD estimates of the three models for radiosonde station 01241 over the
 427 year 2015.

428



429 5 Conclusions

430 The complexity of spatio-temporal variations makes the modelling of tropospheric
431 ZWD difficult. In this paper, the characteristics of vertical variation of wet delay are
432 analysed. The troposphere is divided into three height intervals: below 2 km, 2 km to 5
433 km, and 5 km to 10 km according to different trends (10 km is assumed to represent the
434 empirical tropopause). A quadratic polynomial and two exponential functions are used
435 to describe the variation of wet delay within each of the three intervals. Based on the
436 monthly mean data of ECMWF ZWD from 2001 to 2010, a global ZWD model with
437 spatial resolution of $5^\circ \times 5^\circ$ was established with height fitting followed by periodic
438 fitting. Using the ECMWF ZWD data for 2015, the annual average RMS errors in the
439 HZWD model are 23.8 mm, 13.1 mm, and 2.6 mm in the below 2 km, 2 km to 5 km,
440 and 5 km to 10 km height intervals, respectively, which is far superior to the
441 performance of the UNB3m model. Compared to the currently most accurate wet delay
442 empirical model (the GPT2w model), the precisions within the three height intervals
443 improved by 6%, 6%, and 32%, respectively. The testing results of radiosonde data
444 from 318 stations in 2015 show that the annual average RMS errors of the HZWD
445 model are 30.1 mm, 15.8 mm, and 3.5 mm, which are 2%, 5%, and 33% better than
446 those of the GPT2w model, respectively. Compared with the GPT2w, and UNB3m,
447 models, the HZWD model offers the highest spatio-temporal stability.

448 The HZWD model offers good precision stability in the vertical direction and can
449 meet the requirements of ZWD correction at different heights within the troposphere;
450 however, it can be seen that neither the HZWD, nor the GPT2w, models, *i.e.*, those non-
451 meteorological parameter-based models, performed well in the lower region of the
452 troposphere. In addition, compared with the GPT2w model, HZWD model is a closed
453 model with a limitation to facilitate on-site meteorological observations. Further
454 research is required to assess the variation in and factors influencing of the wet delay
455 and explore the possibility of incorporation of on-site meteorological data.

456

457 *Acknowledgements:* The authors would like to thank the ECMWF and IGRA for



458 providing relevant data. This research was supported by the National Key Research and
 459 Development Program of China (2016YFB0501803) and the National Natural Science
 460 Foundation of China (41574028) and Key Laboratory of Geospace Environment and
 461 Geodesy, Ministry of Education, Wuhan University (16-02-03).

462

463 **References**

- 464 Askne, J., & Nordius, H. (1987). Estimation of tropospheric delay for microwaves from surface
 465 weather data. *Radio Science*, 22(3), 379-386.
- 466 Bevis, M., Businger, S., Herring, T. A., Rocken, C., Anthes, R. A., & Ware, R. H. (1992). GPS
 467 meteorology: Remote sensing of atmospheric water vapor using the Global Positioning System.
 468 *Journal of Geophysical Research: Atmospheres*, 97(D14), 15787-15801.
- 469 Böhmer, J., Möller, G., Schindelegger, M., Pain, G., & Weber, R. (2015). Development of an improved
 470 empirical model for slant delays in the troposphere (GPT2w). *GPS Solutions*, 19(3), 433-441.
- 471 Collins, P., Langley, R., & LaMance, J. (1996). Limiting factors in tropospheric propagation delay
 472 error modelling for GPS airborne navigation. *Proc. Inst. Navig. 52nd Ann. Meet*, 3.
- 473 Davis, J. L., Herring, T. A., Shapiro, I. I., Rogers, A. E. E., & Elgered, G. (1985). Geodesy by radio
 474 interferometry: Effects of atmospheric modeling errors on estimates of baseline length. *Radio*
 475 *science*, 20(6), 1593-1607.
- 476 Hopfield, H. S. (1971). Tropospheric effect on electromagnetically measured range: Prediction from
 477 surface weather data. *Radio Science*, 6(3), 357-367.
- 478 Jin, S., Park, J. U., Cho, J. H., & Park, P. H. (2007). Seasonal variability of GPS - derived zenith
 479 tropospheric delay (1994 - 2006) and climate implications. *Journal of Geophysical Research:*
 480 *Atmospheres* (1984 - 2012), 112(D9).
- 481 Krueger, E., Schueler, T., Hein, G. W., Martellucci, A., & Blarmino, G. (2004, May). Galileo
 482 tropospheric correction approaches developed within GSTB-V1. In *Proc. ENC-GNSS* (Vol. 1619).
- 483 Krueger, E., Schueler, T., & Arbesser-Rastburg, B. (2005). The standard tropospheric correction
 484 model for the European satellite navigation system Galileo. *Proc. General Assembly URSI*.
- 485 Lagler, K., Schindelegger, M., Böhmer, J., Krásný, H., & Nilsson, T. (2013). GPT2: Empirical slant
 486 delay model for radio space geodetic techniques. *Geophysical research letters*, 40(6), 1069-1073.



- 487 Leandro, R., Santos, M. C., & Langley, R. B. (2006, January). UNB neutral atmosphere models:
488 development and performance. In Proceedings of ION NTM (Vol. 52, No. 1, pp. 564-73).
- 489 Möller, G., Weber, R., & Böhm, J. (2014). Improved troposphere blind models based on numerical
490 weather data. *Navigation*, 61(3), 203-211.
- 491 Rózsa S Z. Uncertainty considerations for the comparison of water vapour derived from radiosondes
492 and GNSS[M]/Earth on the Edge: Science for a Sustainable Planet. Springer Berlin Heidelberg,
493 2014: 65-78.
- 494 RTCA (2016), Minimum Operational Performance Standards For Global Positioning
495 System/Satellite-Based Augmentation System Airborne Equipment, Radio Technical Commission
496 for Aeronautics, SC-159, publication DO-229E, Washington, D. C.
- 497 Saastamoinen, J. (1972). Introduction to practical computation of astronomical refraction. *Bulletin*
498 *Géodésique* (1946-1975), 106(1), 383-397.
- 499 Schüller, T. (2014). The TropGrid2 standard tropospheric correction model. *GPS solutions*, 18(1),
500 123-131.
- 501 Song, S., Zhu, W., Chen, Q., & Liou, Y. (2011). Establishment of a new tropospheric delay
502 correction model over China area. *Science China Physics, Mechanics and Astronomy*, 54(12), 2271-
503 2283.
- 504 Zhao J Y, Song S L, Chen Q M, et al. (2014). Establishment of a new global model for zenith
505 tropospheric delay based on functional expression for its vertical profile. *Chinese J. Geophys.* (in
506 Chinese), 57(10), 3140-3153.
- 507